JOURNAL OF APPLIED ELECTROCHEMISTRY 26 (1996) 529–535

Magnetic properties and microstructure of electrodeposited Fe–P amorphous alloy

K. KAMEI, Y. MAEHARA

Advanced Technology Research Laboratories, Sumitomo Metal Industries Ltd, Fuso-cho 1-8 Amagasaki 660 Japan

Received 30 January 1995; revised 14 October 1995

Electrodeposited Fe–P amorphous alloy has been characterized in terms of magnetic properties and the microstructure. The Fe–P electrodeposits show amorphous structure with phosphorus contents of about 20 at%. The formation of the amorphous structure depends mainly on the phosphorus content. The amorphous Fe–P alloy shows typical soft magnetic properties such as low coercive force and high permeability. The coercive force (*Hc*) decreases with the low temperature annealing, and the lowest *Hc* is about 0.05 oersted. This reduction in *Hc* can be attributed to structural relaxation. The amorphous phase is crystallized at temperatures above 300 °C accompanying a drastic increase in *Hc*. The stable crystalline phase is Fe_3P.

1. Introduction

Magnetic thin films have been the subject of many studies, since they are the key head materials for the fabrication of high density recording systems [1, 2]. In terms of manufacture of the thin film heads, electrodeposition combined with microlithography [3–5] is a much more economical and practically applicable technique than sputter deposition. Among various soft magnetic materials that can be processed by electrodeposition, permalloy is now a standard head material [5].

The only disadvantage of permalloy is its low saturation magnetism, which is usually less than 1.0 T. Since the head's ability to record is mainly proportional to the pole material's saturation magnetism, it is essential to increase the thickness of permalloy film to obtain a higher record field suitable for high density recording. It is, however, presently difficult to control the compositional fluctuation in thick electrodeposited permalloy film.

Thus, the establishment of electrodeposition techniques for new pole materials having high saturation magnetization is crucial for high density recording. Recently, several types of electrodeposited alloys with high saturation magnetization (>1.0 T) have been studied [6, 7]. However, the electrodeposition of amorphous magnetic alloys, which have been known as the superior soft magnetic material, has not been intensively studied.

Fe-base amorphous alloys show high saturation magnetism in addition to their soft magnetism that arises from their noncrystalline structure. These alloys are basically formed by the rapid quench method and thereby various multicomponent amorphous magnetic alloys have been developed. This rapid quench method, suitable for fabricating thick ribbons, is rarely applicable to thin film deposition. Although the electrodeposition technique is unsuitable for obtaining a multicomponent alloy, it can easily form binary alloys such as Fe–X. The Fe–P amorphous alloy is one example of such a binary system, and several studies on electrodeposited Fe–P amorphous alloy have been carried out. Logan *et al.* conducted Mössbauer spectroscopy and EXAFS analysis [8–10] to investigate the structure of Fe–P metallic glasses. They also examined the low-temperature electrical resistance of the amorphous Fe–P alloy. Vitkova *et al.* established the optimum condition for the electrodeposition of Fe–P amorphous alloy from the sulfate electrolytes with additives [11]. The soft magnetic properties and their dependence on microstructure, however, are still not fully understood.

In the present study we have examined the magnetic properties, such as coercive force, saturation magnetism and high frequency permeability, and studied the effects of various electrodeposition conditions on these magnetic properties and the microstructure. We have also studied the thermal stability of the amorphous phase and the variations of magnetic properties due to thermal treatment.

2. Experimental details

The electroplating bath was an aqueous solution of $FeSO_4.7H_2O$ and $NaH_2PO_2.H_2O$. The concentration of $FeSO_4.7H_2O$ was 0.1 M and that of $NaH_2PO_2.H_2O$ was chosen in a range from 0 to 0.15 M. The ratio of these solutes was varied so that the effects of the solute concentration on the P concentration of the deposited film could be examined. The pH of the plating bath was adjusted to 2.0 by adding sulfuric acid or sodium hydroxide before the deposition. The temperature of the bath was kept at 50 °C.

Two types of substrates were used: pure copper sheets (40 mm × 160 mm × 0.4 mm) and austenitic

0021-891X

stainless steel sheets (40 mm × 160 mm × 1.0 mm). The deposition area was 40 mm × 40 mm and the other parts of the substrates were shielded by insulating tape. The copper sheets were degreased by the anodic electrolysis in a solution of 10% NaOH, then immersed in a solution of 10% H_2SO_4 for 1 min. The stainless sheets were mirror finished by electrolytic polishing using chromic acid solution.

Plating was carried out galvanostatically with a current density of 500 A m^{-2} in a 700 ml plastic container. The anode and cathode were positioned vertically at the centre of the cell. The distance between them was 1 cm. The anode was a 40 mm × 160 mm × 0.4mm platinum sheet with the same deposition area as the cathode. The plating bath was agitated by magnetic stirrer with stirring rate of 800 rpm. After deposition, the cathodes were immediately removed from the plating bath; they were then rinsed in distilled water and dried in air. Finally, they were sectioned into 1 cm × 1 cm plates and used for the X-ray diffractometry and measurement on the magnetic properties. Thick (about 50 μm) Fe–P alloys were also deposited on stainless steel sheet and were mechanically peeled off the substrates and employed in the X-ray diffractometry, TEM examination and differential scanning calorimetry (DSC).

The coercive force (*Hc*) was measured by using a conventional *Hc* meter. The saturation magnetism was measured by a vibrating specimen magnetometer (VSM). The high frequency magnetic inductance was measured by an impedance analyser. The structural variation of the Fe–P foil due to annealing was characterized by X-ray diffraction (target Co) and a TEM. TEM specimen for the plan-view observation was prepared by percolating the thick foils with conventional twin jet polishing technique. The cross-sectional TEM specimen was prepared by using an ion milling system. The crystallization behaviour of the amorphous Fe–P foil was investigated by DSC with a heating rate of 20 °C min^{-1}. The P content of the deposited film was analysed by induced coupled plasma (ICP) spectroscopy.

3. Results

3.1. *Properties of as-deposited film*

Figure 1 shows the P content of the deposits as a function of that of the plating solution. $[P]_f$ in Fig. 1 denotes the atomic percentage of P in the deposited film, whereas $[P]_s$ denotes the P content in the solution, calculated from the value of $[NaH_2PO_2.H_2O]/([NaH_2PO_2.H_2O]+[FeSO_4.7H_2O])$. In Fig. 1 $[FeSO_4.7H_2O]$ had a constant value of 0.1 M. The $[P]_f$ increases with $[P]_s$ and shows a maximum at a P content around 20 at% when $[P]_s$ is about 40%. This behaviour, given in Fig. 1, was seen at various values of $[FeSO_4.7H_2O]$ and current density, i.e. the alloy approximately presented by Fe(80)P(20), was likely to be formed over a rather wide range of deposition conditions. However, we found it difficult to control the P content

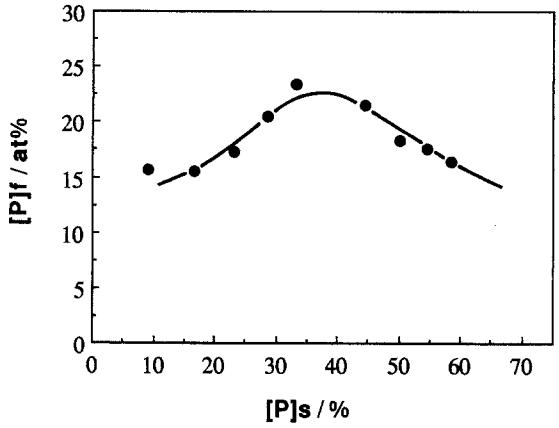

Fig. 1. The P content of the deposited film as a function of that of the plating solution. $[P]_f$: Atomic percentage of P in the deposited film. $[P]_s$: P content in the solution and was calculated from the value of $[NaH_2PO_2.H_2O]/([NaH_2PO_2.H_2O]+[FeSO_4.7H_2O])$. $[FeSO_4.7H_2O]$ was a constant value of 0.1 M and the current density was 500 A m^{-2}.

in the deposits precisely. $[P]_f$ always showed small fluctuations of about 1 to 2 at%. Even in a single specimen there were spatial variations of P content, which might affect the coercive force significantly.

Figure 2 shows the variation of the X-ray diffractogram of the deposits as a function of its P content. As the P content increases, the (1 1 0) α-Fe peak becomes broader showing that amorphous phases are formed. This broadening (i.e. amorphization) occurred at a P content of about 17–24 at%. These amorphization contents coincide well with that of the eutectic point for the Fe–P binary phase diagram [12], which has also been claimed in earlier work [13–15].

Figure 3 shows a cross-sectional TEM micrograph of the electrodeposited Fe–P foil of which the P content was about 20 at%. The foil exhibits homogeneous contrast indicating that there were no crystalline phases. The electron diffraction pattern from the foil was a hollow ring, which is typical of an amorphous structure as shown by the arrow in Fig. 3(b). The interface between Fe–P and Cu substrate is very sharp

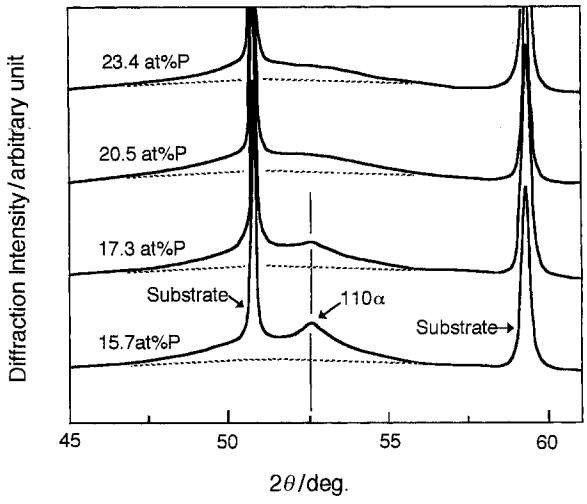

Fig. 2. X-ray diffractogram of the deposits as a function of $[P]_f$. (1 1 0) α-Fe peak becomes broader as the P content increases. Dotted line shows the background intensity.

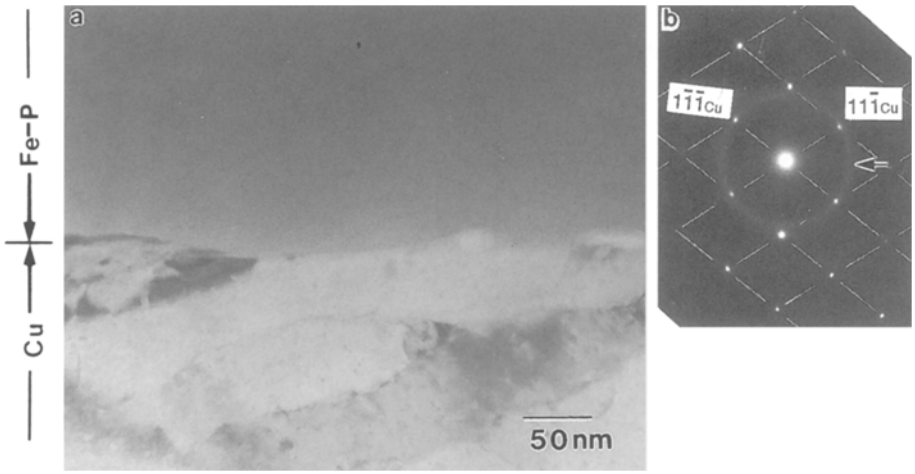

Fig. 3. Cross-sectional TEM micrograph showing the amorphous structure of electrodeposited Fe-20 at% P foil on a Cu substrate. (a) Bright image of a region near the Fe–P/Cu interface. (b) Electron diffraction pattern. Arrow shows the halo ring from Fe–P.

showing that the amorphization occurs at the early stage of the deposition.

Figure 4 shows the effects of P content of the deposits on their coercive force (*Hc*). *Hc* shows a minimum at around 20 at% P content. The minimum is obviously at the amorphization composition. It should be noted that the data are scattered. This variation may be due to the fluctuation of P content in the film as already mentioned. The typical *B–H* curve for the amorphous Fe–P alloy is shown by Fig. 5. The vertical axis shows the magnetization of the film in e.m.u.'s and the saturation magnetism (σ_s) being about 200 e.m.u. g^{-1}. This σ_s is a quite large value compared with permalloy whose σ_s is typically 100 e.m.u. g^{-1}. Figure 6 shows the variation of permeability as a function of frequency. For comparison, the behaviour of the permeability of the electrodeposited permalloy [16, 17] is shown in the Figure. The Fe–P amorphous film has a rather high permeability, even at the high frequency, although its value is lower than that of the electrodeposited permalloy film.

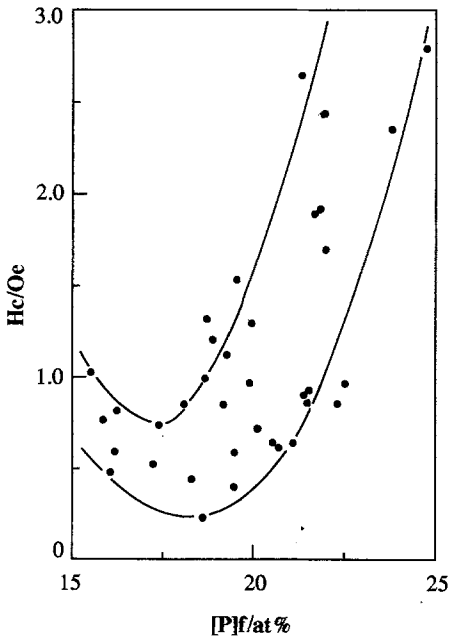

Fig. 4. Effects of P content of the deposits on their coercive force (*Hc*).

3.2. *Variation of magnetic property of amorphous Fe–P during annealing*

Figure 7 shows a DSC spectrum of the amorphous Fe–P film. The spectrum shows a very weak peak at about 300 °C and a strong exothermic peak at 400 °C. The main peak apparently indicates the crystallization into intermetallic phases, since the rapidly quenched Fe–P amorphous alloy shows a similar crystallization peak at 400 °C. The weak peak may correspond to crystallization into supersaturated b.c.c. phase, which is hardly observed in the rapid-quenched Fe–P amorphous structure [18]. Figure 8 shows the variation of *Hc* as a function of the annealing time and temperature. *Hc* decreases from about 1.0 to 0.2 oersted as the temperature increases from 200 to about 250 °C. It should be noted that this drastic change in *Hc* occurs at a temperature below the crystallization temperature. Above 250 °C, *Hc* increases rapidly with increasing annealing temperature, which is apparently due to crystallization into the b.c.c. phase. As 250 °C seems to be the appropriate temperature to decrease the *Hc* to its minimum value, we examined the effects of annealing time on the variation of *Hc* at that temperature. Typical behaviour is shown in Fig. 9. Although the initial value of *Hc* varies due to the fluctuation in P content, *Hc* decreases with annealing time and reaches minimum value after 1 h annealing. The lowest value among several annealed specimens is about 0.05 oersted, which is a sufficiently low value for a thin magnetic head material. The behaviour of *Hc* during the annealing at 250 °C differ from specimen to specimen and seems to depend on the *Hc* value of the as-deposited Fe–P film.

This annealing at 250 °C does not change the microstructure when observed by TEM and X-ray diffractogram as shown in Fig. 10. Even after the annealing for 1.0×10^5 s at 250 °C, the structure of the deposits is still amorphous. However, it should be noted that the line shape of the hollow peak about 52° sharpens

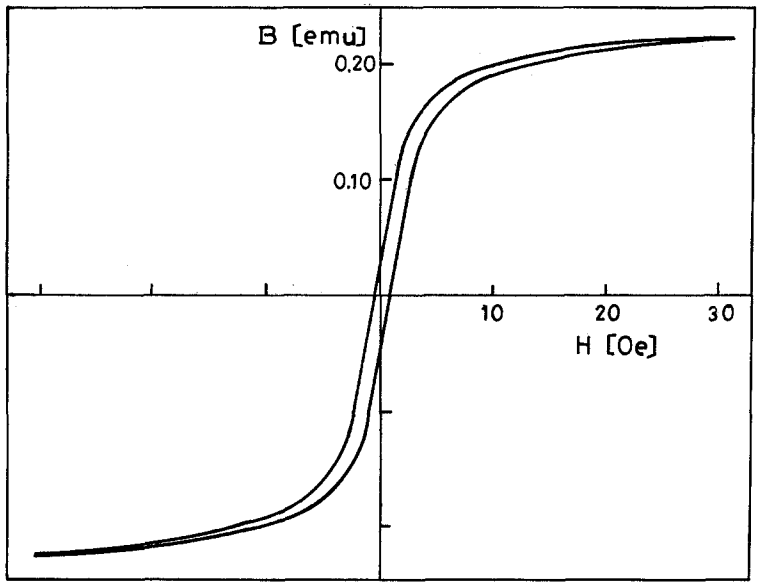

Fig. 5. Typical B–H curve for amorphous Fe–P alloy.

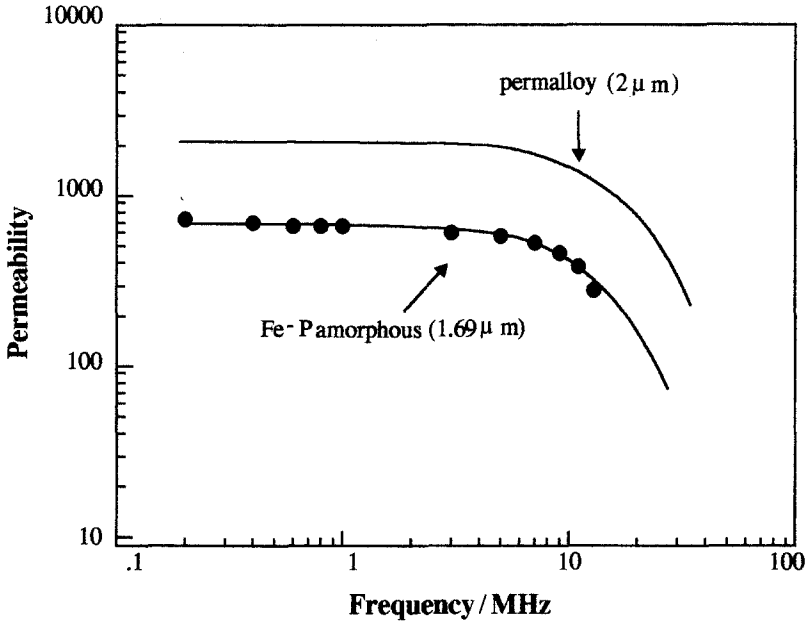

Fig. 6. Variation of permeability as a function of frequency.

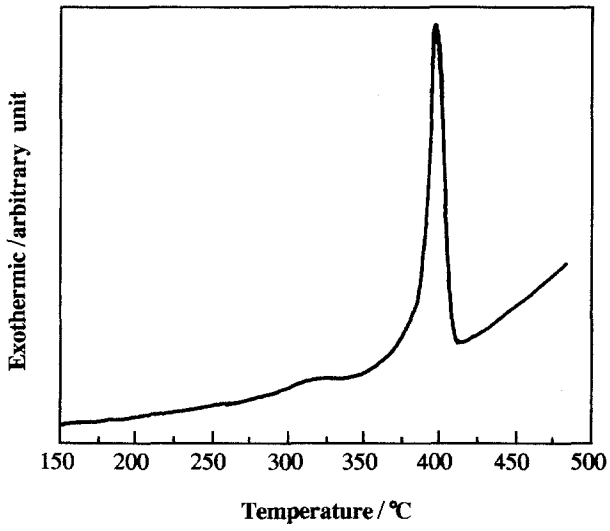

Fig. 7. DSC spectrum of the amorphous Fe–P film.

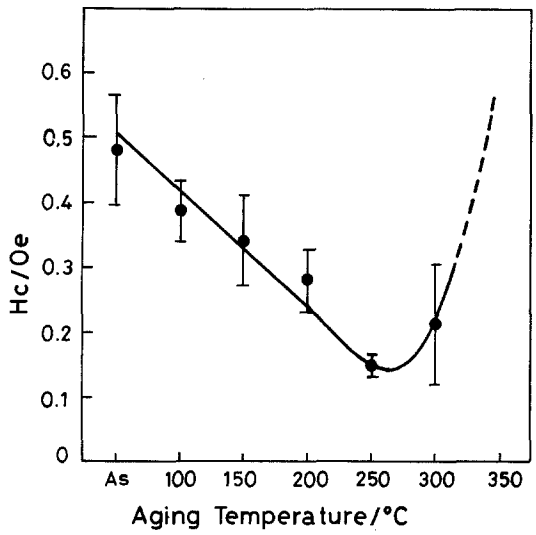

Fig. 8. Variation of Hc as a function of ageing temperature.

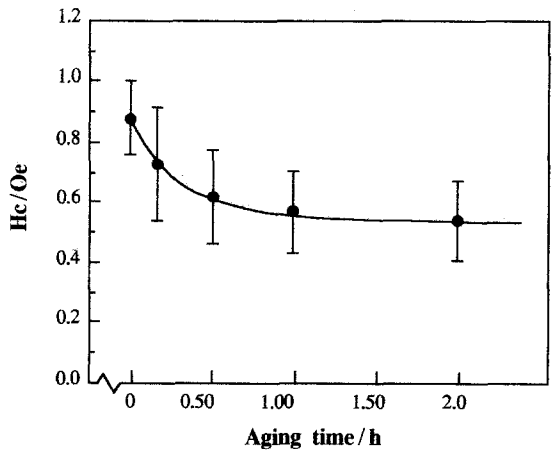

Fig. 9. Effects of ageing time on variation at *Hc* at 250 °C.

with annealing, as seen in the diffraction pattern in Fig. 10. The FWHM in the X-ray diffractogram decreased from 24° to 20° (Fig. 10).

Figure 11 shows the variation of the X-ray diffractogram as a function of annealing temperature. This series clearly shows the crystallization into α-Fe + Fe_3P phases at 400 °C. The structure of intermetallic compounds obtained finally, however, depends significantly on the initial P content of the amorphous Fe–P film, and some of the Fe–P film shows crystallization into α-Fe plus a complicated ordered phase of which the exact structure is unknown.

4. Discussion

The coercive force of the as-deposited Fe–P amorphous film is typically 0.5 oersted, which is comparable with that of electrodeposited permalloy. The exact value of the coercive force is in a range between 0.1 and 1.0 oersted. It also varies spatially in a film. This fluctuation in the coercive force always occurs even under the same deposition conditions. Since the P content in the film also shows similar behaviour, the *Hc* fluctuation may be due to the instability of the P content distribution in the film. In our experiment, the plating solution was agitated using a magnetic stirrer. Therefore, the solution flow conditions are complex and might cause spatial variation of the P content in the film. It should be noted here that both P content and *Hc* varied with distance between the electrodes. This 'distance' effect may indirectly show the effects of flow conditions. It is interesting that the Fe–P film of which the P content is about 20 at% was stably obtained over rather wide solution composition ranges and current densities. There appears to be a mechanism that facilitates the codeposition of Fe and P in the ratio of about 80 : 20.

Crystallization occurs in a single stage, as for melt-quenched Fe–P amorphous sheets. However, it should be noted that the very weak peak can be seen at around 300 °C. This first peak corresponding to the crystallization into the supersaturated b.c.c. phase

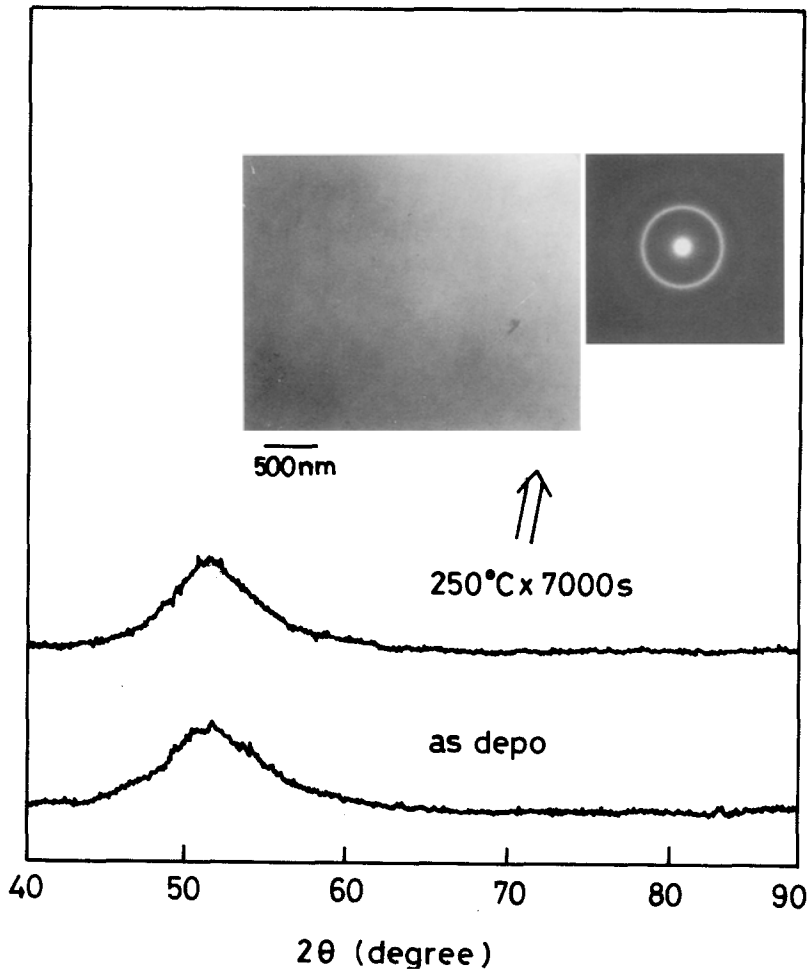

Fig. 10. TEM micrograph and X-ray diffractogram of as-deposited and annealed (for 7000 s at 250 °C) Fe–P film.

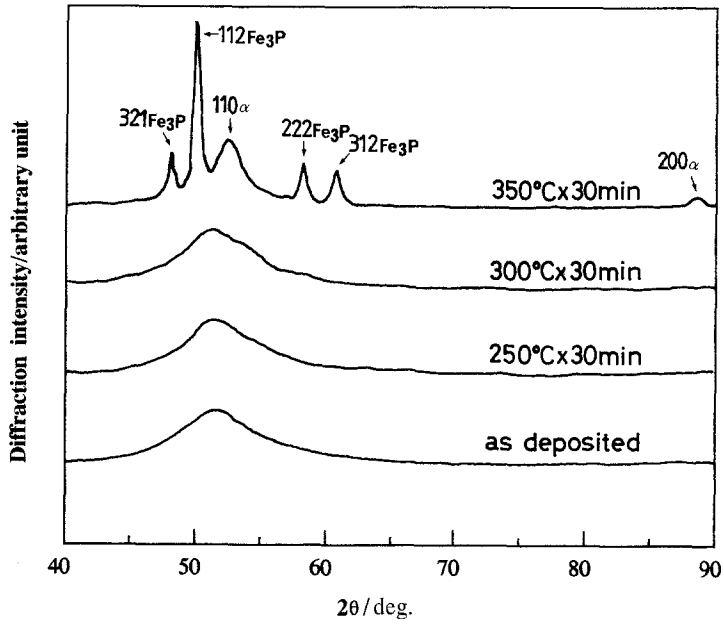

Fig. 11. Variation of X-ray diffractogram as a function of annealing temperature.

was only observed for our Fe–P electrodeposited amorphous film. Since the melt quenched Fe–P amorphous state shows a single stage crystallization clearly, our results may indicate that the microstructural properties such as short range orders in the amorphous film differ between the electrodeposited and the melt quenched film. The intermetallic compound (IMC) that appears at the second crystallization stage at around 400 °C can be attributed to the Fe_3P phase. For some specimens, different kinds of IMC, of which the structure is unknown, were also seen. These are metastable phases and the determination of their exact structure requires further studies by TEM. A typical example of such studies for a rapidly solidified Fe–B amorphous alloy was shown by Duhaj and Hanic [19, 20].

The coercive force is improved by low temperature annealing. Apparently this annealing does not accompany crystallization, as shown by X-ray diffraction and TEM. Therefore, this change in *Hc* is due to the structural relaxation ascribed to the redistribution of free volume [21]. As the result of the structural relaxation, the coercive force decreased to 0.05 oersted. This value of *Hc* is quite low and comparable with that of the rapidly quenched one. The amorphous Fe–P also shows high magnetic permeability of about 800 for the frequency range 0.1 to 1 MHz. This is due to the relatively high electrical resistance of the Fe–P system because the resistance reduces the eddy current loss during high frequency magnetization. The most advantageous property of this Fe–P system is its high saturation magnetism which is typically 200 e.m.u. g^{-1}; this is rarely achieved by permalloy electrodeposits.

One of the problems for the application of this material to the real head pole devices might be its high magnetostriction coefficient. Although the exact value of the saturation magnetostriction coefficient has not been determined in this study, it is expected to be rather high considering the result of the rapid quenched Fe–P system. The other problem is that this system has a high Fe content. Hence it is more likely to be corroded in various environments compared with other systems such as permalloy and Sendust, which contains more chemically stable elements such as Ni, Al and Si. This Fe–P system is, however, the one model for the high saturation pole material. We believe that these advantages can be improved by adding a third or fourth element to the system.

5. Conclusion

The structure and the magnetic properties of Fe–P amorphous electrodeposits have been investigated. The results obtained are as follows:

(i) The electroplated Fe–P amorphous film is obtained at the composition of 20 at% P.
(ii) The coercive force of the as-deposited film is typically 0.2–0.3 oersted with a saturation magnetism of about 200 e.m.u. g^{-1}. The film also shows rather high permeability, even at a high frequency such as 10 MHz.
(iii) Low temperature annealing reduces the coercive force to less than 0.1 oersted. This reduction may be due to structural relaxation.
(iv) The amorphous Fe–P crystallize into the supersaturated b.c.c. phase at 300 °C and into the Fe_3P phase at 400 °C accompanied by a drastic increase in the coercive force.

Acknowledgements

The authors would like to thank S. Uenoya, K. Hanafusa and Y. Itoh for technical assistance. The authors also wish to express appreciation to Dr S. Watanabe for his encouragement and support.

References

[1] T. Jagielinski, *MRS Bulletin* **5** (1990) 36.
[2] J. Lemke, *ibid.* **15** (1990) 31.
[3] U. Wagner and A. Zilk, *IEEE Trans. Mag.* **18** (1982) 877.

[4] J. Horkans, *J. Electrochem. Soc.* **128** (1981) 45.
[5] L. T. Romankiw and T. A. Palumbo, Proceedings of the Conference on 'Electrodeposition Technology, Theory and Practice' (edited by L. T. Romankiw and D. R. Turner), vol. **87–17** (1987) p. 25.
[6] M. Sano, T. Imagawa, S. Narishige, M. Hanazono and Y. Sugita, INTEREMAG '87 DD02 Tokyo, Japan (1987).
[7] S. H. Liao, *IEEE Trans. Magn.* **26** (1990) 328.
[8] J. Logan, *Pays. Star. So. (a)* **32** (1975) 361.
[9] J. Logan and E. Sun, *J. Non-Cryst. Solids* **20** (1976) 285.
[10] Idem, *ibid.* **21** (1976) 151.
[11] S. T. Vitkova, M. Kjuchukova and G. Raichevski, *J. Appl. Electrochem.* **18** (1988) 673.
[12] P. M. Hansen, 'Constitution of Binary Alloys,' McGraw-Hill (1958).
[13] M. Naka and T. Masumoto, 1684th report of the Research Institute for Iron, Steel and Other Metals (1979) p. 118.
[14] T. Watanabe and Y. Tanabe, *Plat. Surf. Technol.* **32** (1981) 600.
[15] A. Brenner, D. E. Couch and E. K. Williams, *J. Res. National Bureau of Standards* **44** (1950) 109.
[16] H. Kamimura, private communication.
[17] J. S. Y. Feng and D. A. Thompson, *IEEE Trans. Magn.* **13** (1977) 1521.
[18] M. Naka and T. Masumoto, 1684th report of the Research Institute for Iron, Steel and Other Metals.
[19] P. Duhaj and F. Hanic, *Phys. Stat. Sol. (a)* **62** (1980) 719.
[20] *Idem, ibid.* **76** (1983) 467.
[21] S. Kobayasi and S. Takeuchi, *J. Phys. F: Met. Phys.* **14** (1984) 23.